Numerical studies of the interstellar medium on galactic scales

Pelupessy, F.I.

Chapter 6

Molecular gas and star formation

Abstract

We present models of the coupled evolution of the gaseous and stellar content of dwarf galaxies using a hybrid N-body/hydrodynamics code and a Jeans mass criterion to describe the onset of star formation from gas. We now incorporate for the first time the formation of H_2 gas as part of the model. We do so by formulating a sub-grid model for molecular clouds, assumed to obey well-known scaling relations, and solving for the HI↔H_2 balance set by the H_2 formation on dust grains and its FUV-induced photodissociation. This then allows the tracking of the evolution of the molecular gas of galaxies seamlessly along with that of its precursor cold neutral medium HI gas. The thermal and dynamic evolution of gas as dense as $\sim 2 \times 10^2$ cm^{-3} and as cold as $\mathrm{T_k} \sim 40$ K (where most of the HI→H_2 transition is expected) is probed in our simulations. We are thus able to identify the molecular regions of the interstellar medium during the evolution of a typical dwarf galaxy. We find a significant dependence of the HI→H_2 transition and the resultant H_2 gas mass on the ambient metallicity and the H_2 formation rate, results we expect to be valid in all other types of galaxies for which the dense and cool HI precursor and the resulting H_2 gas phases are currently inaccessible by high resolution numerical studies (e.g. large spirals).

6.1 Introduction

Stars form in molecular clouds, and most stars form in the large complexes of giant molecular clouds (GMCs). A general theory to predict the location and amount of star formation in galaxies does not exist yet. The global drivers of star formation are generally sought in large scale processes that can form concentrations of HI gas (Elmegreen 2002), for example gravitational instabilities in disk galaxies, or compression by galaxy interactions or mergers. These concentrations of neutral gas are then

assumed to be the sites of molecular cloud and ultimately star formation. Computer simulations of galaxies have followed this lead and base their star formation model usually on the local density directly using a Schmidt law (Mihos & Hernquist 1994, Springel 2000, Semelin & Combes 2002), or on the consideration of gravitational instability using a Jeans mass criterion (Katz 1992, Gerritsen & Icke 1997), and none explicitly consider molecular gas.

The interstellar medium (ISM) consists of gas with a wide ranging properties, from cold, dense molecular clouds to the cold and warm neutral medium (CNM, WNM) and the hot ionized medium intermixed in fractal-like structures. The physical processes governing the state of the ISM have been progressively identified in the last few decades, but the precise working of these, amongst which various heating, cooling and ionization processes, is still an area of active research (Vázquez-Semadeni 2002). Most galactic scale simulations include only one phase, best thought of as the warm neutral medium (Katz 1992, Navarro & White 1993, Springel 2000). Some authors have tried to include more physics to model a two phase medium (Gerritsen & Icke 1997, Gerritsen & de Blok 1999), or incorporated an empirical model for a multiphase ISM (Springel & Hernquist 2002, Semelin & Combes 2002, Andersen & Burkert 2000). The inclusion of the molecular component into simulations of the ISM of galaxies on galactic scale is generally not attempted, and so such simulations cannot be compared directly to the numerous observations of H_2 gas distribution in galaxies (as revealed by its tracer molecule CO).

Thus, apart from the obvious fallacy of forming stars out of atomic gas, the absence of molecular gas deprives the simulation of a valuable diagnostic tool that one could use to constrain the many free parameters that are part of this type of modelling: molecular gas in galaxies is observationally well studied and a host of empirical relations have been established between molecular gas and star formation. For example the Schmidt law has been demonstrated to be a much tighter relation for molecular, rather than HI gas (Wong & Blitz 2002). Recently, CO observations are beginning to yield complete surveys of metal-rich molecular gas of nearby galaxies (Engargiola et al. 2003, Mizuno et al. 2001, Helfer et al. 2001, Regan et al. 2001). The catalogues of molecular clouds from these works can be matched against Hα observations, which yields information regarding lifetimes of giant molecular clouds. On a more detailed level, studies of molecular gas in the dense shells around superbubbles in for example the Large Magellanic Cloud (LMC) are used to unravel the star formation sequence (Yamaguchi et al. 2001). Thus, while the study of the relation between molecular gas and star formation is part and parcel of observational studies of galaxies, the theoretical approach of study of these complex systems by numerical simulation lacks such a possibility, simply because of the computational demands of following the formation of molecules from first principles.

For primordial gas, where H_2 forms in the gas phase and no radiation sources are present, simulations have followed the H_2 chemistry (Abel 1997), but these are not applicable to current star forming galaxies. Some pioneering work to include H_2 into simulations of star forming spiral galaxies has been done by Hidaka & Sofue (2002) but they did not consider a time dependent HI$\rightarrow$H$_2$ transition, which as we will argue below, is essential. In this chapter, we will describe a method to incorporate a realistic H_2 formation criterion into simulations of galaxies. It is based on the application of a time-dependent HI$\rightarrow$H$_2$ transition to a sub-grid model for interstellar clouds. This

method allows us to simulate galaxies without omitting an important ISM component which constitutes the "fuel" of all star formation activity in galaxies. We implement our method in an N-body/SPH code - although we want to emphasize that it can be implemented in more general types of code for the simulation of the ISM. First results for dwarf irregulars indicate the critical role of metallicity and the H_2 formation rate on the distribution and total amount of H_2 present. Thus, this work contributes to filling two gaps in the literature. First, the H_2 formation criterion makes a connection between galaxy-sized simulations and molecular cloud theory, making the results of numerous theoretical studies of cloud formation accessible and applicable to such simulations. Secondly, our method can be used to explore the connection between large scale instabilities and the formation of molecular gas complexes. Star formation and molecular gas can then be studied in the dynamic setting of realistic galaxy models that include effects of e.g. spiral density waves, self propagating star formation, galaxy interactions and mergers.

In Section 6.2 we will first give an overview of a simplified version of the theory of H_2 formation and destruction, in sections 6.3 and 6.4 we will discuss the N-body/SPH code we use and the actual implementation of our H_2 criterion, whereafter we present the first results of our modelling in section 6.5.

6.2 H_2 formation and destruction

The formation of H_2 in galaxies has already been studied by Elmegreen (1989, 1993), where the important role of ambient metallicity and pressure has been described. Subsequent efforts to incorporate his approach into analytical models of galactic disks (Honma et al. 1995) or numerical simulations (Hidaka & Sofue 2002) have adopted stationary models, namely once an H_2 formation criterion is satisfied the HI$\rightarrow$$H_2$ transition is set to be instantaneous. The time-dependence of several factors affecting this transition (e.g. the ambient H_2-dissociating radiation field) and the various gas heating and cooling processes were not considered. This seriously restricts the ability of such models to track the evolution of the ISM and particularly its H_2 gas phase. This is because the conditions affecting the HI$\leftrightarrow$$H_2$ equilibrium can vary over timescales comparable to or shorter than that needed for equilibrium to be reached.

Dust grains, when present, are the sites where H_2 mostly forms. The H_2 formation rate $\mathrm{R_f}$ for gas with temperature $\mathrm{T_k}$ and metallicity Z can then be expressed as

$$\mathrm{R_f} = \frac{1}{2}\sigma_\mathrm{d}\langle \mathrm{v_H}\rangle \mathrm{S_H}\gamma_{\mathrm{H_2}} = 3.5\times10^{-18}\mu \mathrm{Z T_k^{1/2} S_H}\gamma_{\mathrm{H_2}}\ \mathrm{cm^3\ s^{-1}}, \quad (1)$$

(e.g. Hollenbach, Werner, & Salpeter 1971; Cazaux & Tielens 2002, 2004). This equation expresses the rate of collisions resulting in H_2 formation of H atoms, having mean velocities $\langle \mathrm{v_H}\rangle$, with interstellar dust particles with effective surface σ_d. The grain surface (and thus the formation rate) is assumed to scale linearly with metallicity Z, $\sigma_\mathrm{d} = \sigma_\mathrm{g}\mathrm{n_g/n} = 4.9\times10^{-22}\mathrm{Z\ cm^2}$, for grain surface σ_g and ratio of grain density to hydrogen density $\mathrm{n_g/n}$. The functions $\mathrm{S_H} = \mathrm{S_H(T_k)}$ and $\gamma_{\mathrm{H_2}} = \gamma_{\mathrm{H_2}}(\mathrm{T_{dust}})$ express the HI grain-sticking , and H_2 formation probability (once HI is on the grain surface) respectively. Laboratory experiments usually constrain only the product $\mathrm{S_H}\gamma_{\mathrm{H_2}}$ for various temperature domains rather than provide any analytical fits for each function

separately (e.g. Pirronello et al. 1997; Katz et al. 1999). The theoretical study of Buch & Zhang (1991) yields a function $\mathrm{S_H} = [1 + (\mathrm{k_B T_k}/\mathrm{E_\circ})]^{-2}$ ($\mathrm{E_\circ}/\mathrm{k_B} = 102$ K) valid for $\mathrm{T_k} \lesssim 300$ K, which we adopt in the present work. We incorporate the uncertainties of the H_2 formation rate into a constant parameter μ. These uncertainties reside mainly in the formation probability, but also in the effective surface for H_2 formation. This surface may be bigger than the value σ_d, which is actually the value for the effective visual extinction cross-section. A value of $\mu = 3.5$ corresponds to the canonical formation rate $\mathrm{R_f} = 3 \times 10^{-17}$ cm^3 s^{-1} (e.g. Jura 1974, 1975), for typical CNM HI gas conditions ($\mathrm{T_k} \sim 100$ K), but values up to $\mu \sim 18$ are not excluded. Early suggestions for a high value of μ emerged from the study of rovibrational infrared lines of H_2 in reflection nebulae (Sternberg 1988), and more recently from the detections of particularly intense H_2 rotational lines with the Infrared Space Observatory (ISO) in photodissociation regions (Habart et al. 2000; Li et al. 2002).

The timescale associated with H_2 formation is (e.g. Goldshmidt & Sternberg 1995)

$$\tau_\mathrm{f} = (2\mathrm{n}\mathrm{R_f})^{-1} = 5 \times 10^7 \left(\frac{\mathrm{T_k}}{100\ \mathrm{K}}\right)^{-1/2} \left(\frac{\mathrm{n}}{10\ \mathrm{cm^{-3}}}\right)^{-1} [\mu \mathrm{Z} \mathrm{S_H}(\mathrm{T_k})]^{-1}\ \mathrm{yrs}, \quad (2)$$

where n and $\mathrm{T_k}$ are the density and temperature of HI. For $\mathrm{n} \sim 50$ cm^{-3} and $\mathrm{T_k} \sim 100$ K, typical of the Cold Neutral Medium HI gas out of which H_2 clouds form, $\tau_\mathrm{f} \sim 10^7$ yrs. This is comparable to the timescales of a wide variety of processes expected to fully disrupt or otherwise drastically alter typical molecular clouds and their ambient environments. Some of the most important ones are star formation, with the disruptive effects of OB associations (e.g. Bash et al. 1977), turbulent dissipation (Stone et al. 1998; MacLow et al. 1998), and inter-cloud clump-clump collisions (Blitz & Shu 1980). The *mean* FUV field driven by the evolution of continously forming stellar populations throughout a galaxy evolves over similar timescales (e.g. Parravano, Hollenbach & McKee 2003), and the same is the case for the ambient pressure environment and its perturbations by passing supernova (SN) induced shocks (e.g. Wolfire et al. 2003). *Hence a realistic model of the HI→H_2 transition in galaxies must be time-dependent.*

6.2.1 Equilibrium molecular fraction

The equilibrium molecular gas fraction per cloud, under a given ambient FUV field, can be estimated by considering the formation/destruction equilibrium for a plane parallel cloud illuminated by a radiation field $\mathrm{G_\circ}$. In equilibrium formation balances destruction, hence

$$\mathrm{R_f n n_1} = \mathrm{G_\circ k_\circ f(N_2) e^{-\tau} n_2} \quad (3)$$

which must hold at any depth. The densities $\mathrm{n_1}$ and $\mathrm{n_2}$ denote the HI and H_2 densities, while the total hydrogen density is $\mathrm{n} = \mathrm{n_1} + 2\mathrm{n_2}$. The H_2 dissociation rate $\mathrm{k_\circ} = 4 \times 10^{-11}$ s^{-1} is normalised for an ambient FUV field in units of the Habing (1968) field value ($\mathrm{G_\circ} = 1$). The factor $\mathrm{f(N_2)}$ is the normalised H_2 self-shielding function which describes the decrease in dissociation rate due to absorption by the molecular column, $\mathrm{N_2}$. Furthermore, $\tau = \sigma(\mathrm{N_1} + 2\mathrm{N_2})$ is the FUV continuum optical depth due to grain extinction, with a dust FUV absorption cross-section $\sigma = \xi_\mathrm{FUV}\sigma_\mathrm{d}$ for $\xi_\mathrm{FUV} = 2 - 4$. Eq. (3) can be converted to a separable differential equation for the

columns N_1 and N_2 (e.g. Goldshmidt & Sternberg 1995) which, when integrated by parts for a uniform cloud, yields an HI transition column density

$$N_{tr}(HI) = \frac{1}{\sigma} \ln\left(1 + \frac{G_\circ k_\circ}{n R_f}\Phi\right). \quad (4)$$

This is the total HI column density marking the HI/H_2 transition zone from the surface of the cloud for a uniform one-side illuminated cloud. The factor Φ is an integral of the self-shielding function over the H_2 column (Goldshmidt & Sternberg 1995), which for $f(N_2) \sim N_2^{-k}$,

$$\Phi = 2^{k-1}\left(N_{ch}\sigma\right)^k \int_0^\infty x^{-k} e^{-x} dx = 6.6 \times 10^{-6} \sqrt{\pi}\, Z^{1/2} \xi_{FUV}^{1/2}, \quad (5)$$

and encompasses the details of the H_2 self-shielding. Its numerical value was obtained for $k = 1/2$ and a characteristic column density of $N_{ch} = 1.75 \times 10^{11}$ cm^{-2} (Jura 1974).

The equation of the HI↔H_2 balance still yields an analytical expression for $N_{tr}(HI)$ for clouds with density profile: $n(r) = n_{ex}(r/R)^{-1}$, with R the cloud radius. Such a profile results from cloud models using a logotropic equation of state (Mclauglin & Pudritz 1996) hence we will refer to them as "logotropic clouds," but the reason we will consider such profiles here is that this is a rough representation of sub-resolution, non-uniform, GMC density structure. For a radial incident interstellar radiation field, such a density profile yields

$$N_{tr}(HI) = \frac{\nu_\circ}{\sigma} \ln\left(1 + \nu_\circ^{-1} \frac{G_\circ k_\circ}{n_{ex} R_f}\Phi\right), \quad (6)$$

where $\nu_\circ = n_{ex} R \sigma \left(1 + n_{ex} R \sigma\right)^{-1}$. For $R \to \infty$ we obtain $\nu_\circ \to 1$ and Eq. (6) reduces to Eq. (4) as expected for uniform density clouds ($n(r) \to n_{ex}$). The visual extinction corresponding to (6) is given by (using the expressions for R_f and ϕ, (1) and (5))

$$A_v^{(tr)} = 1.086 \nu_\circ \xi_{FUV}^{-1} \ln\left[1 + \frac{\nu_\circ^{-1} G_\circ}{\mu S_H(T_k)} \left(\frac{\xi_{FUV}}{Z T_k}\right)^{1/2} \left(\frac{n_{ex}}{135\ \text{cm}^{-3}}\right)^{-1}\right]. \quad (7)$$

It is then easy to show that the H_2 gas mass fraction contained inside the HI transition zone marked by $A_v^{(tr)}$ is given by

$$f_m = \frac{M(H_2)}{M_c} = \left(1 - \frac{4A_v^{(tr)}}{3\langle A_v\rangle}\right)^3, \quad (8)$$

for constant density clouds, and

$$f_m = \frac{M(H_2)}{M_c} = \exp\left[-4\frac{A_v^{(tr)}}{\langle A_v\rangle}\right] \quad (9)$$

for logotropic clouds. Here, $\langle A_v\rangle$ is the average extinction for a spherical cloud measured by an outside observer.

We consider the cloud fraction $\mathrm{f_m}$ to be a measure of the local molecular gas content of the ISM. Here, the implicit assumption is that most of the HI/H_2 gas mass ultimately can be traced in such cloud structures. For CNM HI and the resulting H_2 clouds this is a reasonable assumption. In certain models this is predicted to be the final configuration of any initial gas mass which quickly cools and fragments in an environment of constant "background" pressure (Chièze 1987; Chièze & Pineau des Forêts 1987).

To derive $\mathrm{f_m}$ we need some measure of the average cloud extinction $\langle \mathrm{A_v} \rangle$. The crucial assumption we make in order to derive this is that all unresolved cloud structures in the ISM where the HI/H_2 transition takes place obey the widely observed density-size power law (e.g. Larson 1981). The bulk of the H_2 gas is assembled in Giant Molecular Clouds, the sites of most star formation activity in galaxies, and which are observed to be virialised entities (e.g. Larson 1981, Elmegreen 1989 and references therein). Indeed their well known density/size scaling relation can be readily reproduced from the virial theorem applied for clouds under a given boundary pressure $\mathrm{P_e}$ (Elmegreen 1989). In this case it can be shown that the average H density is given by

$$\langle \mathrm{n} \rangle = \mathrm{n_\circ} \left(\frac{\mathrm{P_e/k_B}}{10^4 \text{ K cm}^{-3}} \right)^{1/2} \mathrm{R_{pc}^{-1}}, \tag{10}$$

where $\mathrm{R_{pc}}$ is the cloud radius in parsecs. The range of the normalising constant $\mathrm{n_\circ}$ (cm^{-3}) can be determined theoretically by choosing a range of plausible polytropic solutions to the cloud density profiles (e.g. Elmegreen 1989), or from the *observed* n-R relations for galactic molecular clouds. The latter approach, after using the scaling relation $\mathrm{n(H_2)} = 1700 \mathrm{R_{pc}^{-\alpha}}$ cm^{-3} reported by Larson (1981) ($\alpha \sim 1$), yields $\mathrm{n_\circ} \sim 1520$ cm^{-3}. In estimating $\mathrm{n_\circ}$ from the observed n-R scaling relation we took into account that for the galactic midplane molecular clouds the outer pressure $\mathrm{P_\circ/k_B} \sim 10^4$ K cm^{-3} , but the boundary pressure on the molecular part of the cloud $\mathrm{P_e} = \mathrm{P_{e,m}} \sim 5\mathrm{P_\circ}$ (Elmegreen 1989). Using (10) we estimate the average extinction of a cloud with radius R as measured from the outside as

$$\langle \mathrm{A_v} \rangle = 2 \mathrm{k_g} \langle \mathrm{n} \rangle \mathrm{R} \sigma_\mathrm{d}, \tag{11}$$

with a geometric factor $\mathrm{k_g} = 2/3$ (for a spherical cloud). After substituting $\langle \mathrm{n} \rangle$ from Eq. (10) we get,

$$\langle \mathrm{A_v} \rangle = 0.22 \mathrm{Z} \left(\frac{\mathrm{n_\circ}}{100 \text{ cm}^{-3}} \right) \left(\frac{\mathrm{P_e/k_B}}{10^4 \text{ K cm}^{-3}} \right)^{1/2}. \tag{12}$$

The cloud boundary pressure is due to thermal and macroscopic motions (Elmegreen 1989), assuming the latter to be isotropic, $\mathrm{P_e}$ can be expressed as

$$\mathrm{P_e} = \mathrm{n_{ex} k_B T_k} + \frac{1}{3} \rho_\mathrm{e} \sigma_\mathrm{vel}^2 = \left[1.085 \mathrm{T_k} + 54 \left(\frac{\sigma_\mathrm{vel}}{\text{km s}^{-1}} \right)^2 \mathrm{K} \right] \mathrm{n_{ex} k_B}, \tag{13}$$

where σ_vel is the 3-dimensional velocity dispersion of the gas due solely to macroscopic motions. From (8), (9), and (12) it is obvious that high pressure gas will tend to be molecular, a result already known from the analytical/steady-state models of the HI→H_2 transition in galactic disks (Elmegreen 1993; Honma et al. 1995).

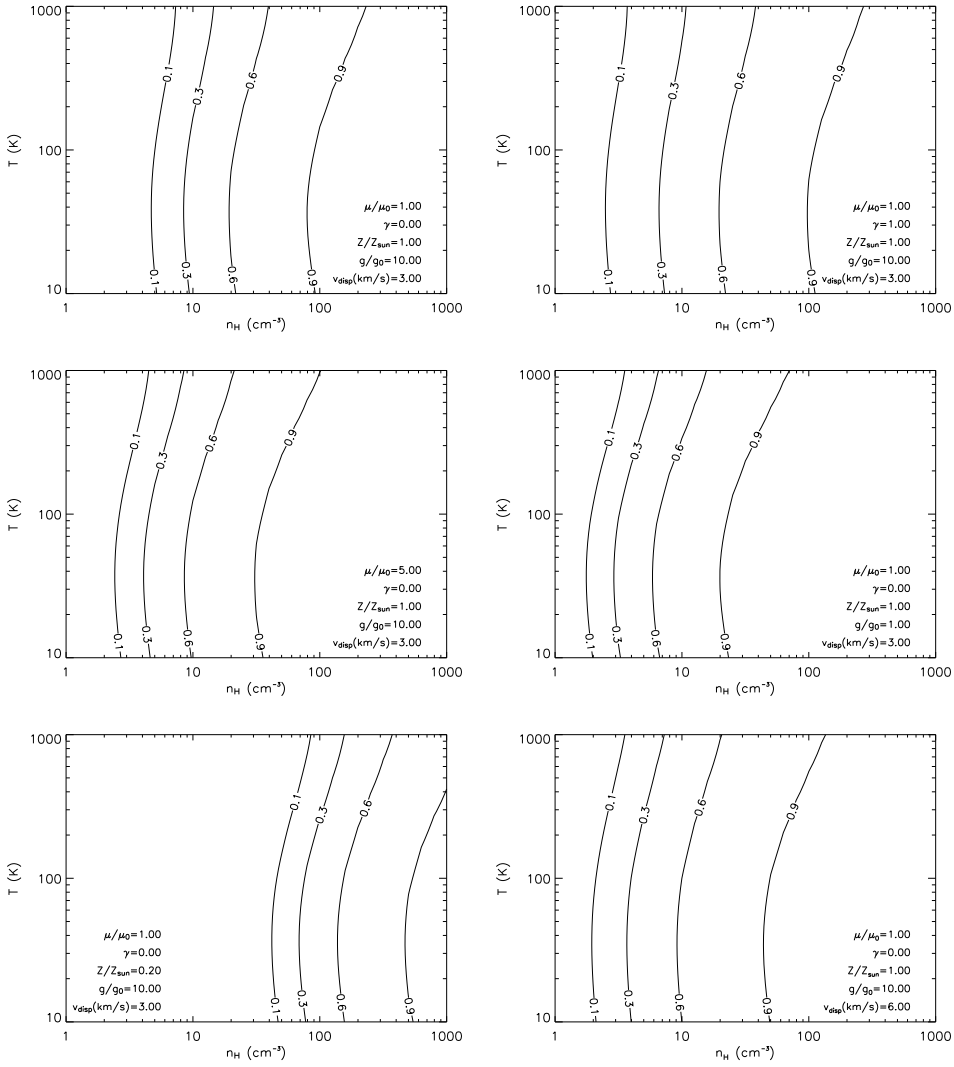

Figure 6.1: The Equilibrium molecular fraction $\mathrm{f_m}$. Plotted are contours of $\mathrm{f_m}$ labelled with the contour value. Above 1000 K the formation rate is taken to be zero. γ indicates the power law index of the cloud density profile ($\mathrm{n} \propto \mathrm{r}^{-\gamma}$), thus $\gamma = 0$ means constant density clouds, $\gamma = 1$ logotropic clouds.

We can now calculate the equilibrium $\mathrm{f_m}$ for a given parcel of interstellar gas of temperature T and density n using Eqs. (8) or (9). Input parameters are the radiation field $\mathrm{G_0}$, metallicity Z, velocity dispersion σ_{vel} and our H_2 formation rate parameter μ. In Fig. 6.1 we have plotted the resulting equilibrium fraction $\mathrm{f_m}$ for a number of typical values of these parameters.

The true equilibrium molecular gas content will most likely be higher than $\mathrm{f_m}$ since the real ISRF incident on GMCs is not radial and thus falls off more rapidly inside the absorbing cloud layers. Higher gas densities that exist deeper in the clouds as part of the considerable spatial and density substructure/clumping observed in the ISM will act to raise the true $\mathrm{f_m}$. In that respect logotropic clouds are more realistic than those with uniform density.

6.2.2 Time-dependence of the HI/H_2 equilibrium

The time dependent HI/H_2 transition can be approximated from the solution of Equation (22) of Goldshmidt & Sternberg (1995), which describes the evolution of the total HI column $\mathrm{N_tr(HI)}$ in the HI→H_2 transition layer of a plane parallel slab of H_2 gas with an impinging dissociating radiation field:

$$\tau_{\mathrm{f}} \frac{\mathrm{d}\sigma \mathrm{N_{tr}(HI,t)}}{\mathrm{dt}} = \mathrm{r_{dis}} \mathrm{e}^{-\sigma \mathrm{N_{tr}(HI,t)}} - \sigma \mathrm{N_{tr}(HI,t)}, \tag{14}$$

where $\tau_{\mathrm{f}} = 1/(2\mathrm{nR_f})$ is the H_2 formation time and the quantity $\mathrm{r_{dis}}$ quantifies the local balance between H_2 dissociation and formation and is given by

$$\mathrm{r_{dis}} = \frac{\mathrm{G_\circ k_\circ}}{\mathrm{nR_f}} \Phi = 2.67 \frac{\mathrm{G_\circ}}{\mu \mathrm{S_H(T_k)}} \left(\frac{\xi_{\mathrm{FUV}}}{\mathrm{ZT_k}} \right)^{1/2} \left(\frac{\mathrm{n}}{50\ \mathrm{cm^{-3}}} \right)^{-1}. \tag{15}$$

The assumption underlying the validity of Eq. (14) is that of an extremely narrow HI/H_2 transition layer, which thus separates the slab into a fully atomic and a fully molecular section. In the case of steady state Eq. (14) reduces to

$$\mathrm{r_{dis}} \mathrm{e}^{-\sigma \mathrm{N_{tr}(HI)}} = \sigma \mathrm{N_{tr}(HI)}, \tag{16}$$

which does not yield $\mathrm{N_{tr}(HI)}$ as expressed in Eq. (4), though solutions of Eq. (16) for $\mathrm{N_{tr}(HI)}$ differ $\lesssim 30\%$. This is not surprising given that Eq. (4) does not involve the approximation of a sharp HI/H_2 transition. It is easy to see at what step of deducing Eq. (4) the assumption of a sharp HI/H_2 transition layer yield the result expressed in Eq. (16). From Goldshmidt and Sternberg (their Equation 2)

$$\mathrm{R_f n dN(HI)} = \mathrm{G_\circ k_\circ f[N(H_2)]} \mathrm{e}^{-2\sigma \mathrm{N(H_2)}} \mathrm{e}^{-\sigma \mathrm{N(HI)}} \mathrm{dN(H_2)}. \tag{17}$$

If not much HI exists within the sharp HI/H_2 transition zone to significantly add up to the total HI transition column density we can replace $\mathrm{e}^{-\sigma \mathrm{N(HI)}}$ by $\mathrm{e}^{-\sigma \mathrm{N_{tr}(HI)}}$ The latter is then treated as a constant of integration over the H_2 column density and kept in the right part of the latter equation yielding Eq. (16).

A fully time-dependent treatment of the HI/H_2 transition is conveniently provided by solving Eq. (14) for $\mathrm{A_{FUV}^{(tr)}} = \sigma \mathrm{N_{tr}(HI,t)}$ and finding the corresponding $\mathrm{f_m(t)}$ from Eq. (8). Although the approximation of a narrow transition layer is not strictly valid, the time dependent solution of the full integro-differential equation would be too costly for use in numerical simulations, and also the uncertainties inherent in our model would not justify the additional expense for the more exact solution.

Analytical approximations of time varying H_2 transition

It is interesting to examine approximate analytical solutions, if only for the reason of checking the more general solution of Eq. (14) in limiting cases. This can be done for two particular domains, namely that of rapidly increasing and rapidly decreasing $\mathrm{A_{FUV}^{(tr)}(t)}$. For $\tau_\mathrm{f}\mathrm{dA_{FUV}^{(tr)}}/\mathrm{dt} \ll 0$ we can approximate Eq. (14) as

$$\frac{\mathrm{dA_{FUV}^{(tr)}}}{\mathrm{dt}} = -\frac{1}{\tau_\mathrm{f}}\mathrm{A_{FUV}^{(tr)}} \Rightarrow \mathrm{A_{FUV}^{(tr)}} = \mathrm{A_{FUV}^{(tr)}(0)e^{-t/\tau_f}}. \tag{18}$$

In the case of $\tau_\mathrm{f}\mathrm{dA_{FUV}^{(tr)}}/\mathrm{dt} \gg 1$, and thus a decreasing molecular mass fraction, we approximate Eq. (14) as

$$\frac{\mathrm{dA_{FUV}^{(tr)}}}{\mathrm{dt}} = \frac{\mathrm{r_{dis}}}{\tau_\mathrm{f}}\mathrm{e^{-A_{FUV}^{(tr)}}} = 2\mathrm{G_\circ k_\circ \Phi e^{-A_{FUV}^{(tr)}}}, \tag{19}$$

hence

$$\mathrm{A_{FUV}^{(tr)}(t)} = \ln\left(\mathrm{e^{A_{FUV}^{(tr)}(0)}} + 2\mathrm{G_\circ k_\circ \Phi t}\right), \tag{20}$$

which in the case of $\mathrm{R_f} = 0$, provides a convenient solution describing the photo-destruction of molecular clouds.

The case of logotropic clouds

Eq. (14) is derived under the assumption of the HI/H_2 transition being sharp and under the assumption of a uniform density. In the case of a radial density profile the latter is no longer the case, but the approximation of a sharp HI/H_2 transition can be maintained. In the case of a logotropic density profile the modification of Eq. (14) (or Eq. (22) of Goldshmidt and Sternberg (1995)) turns out to be particularly simple,

$$\frac{1}{2}\frac{\mathrm{dN(HI,t)}}{\mathrm{dt}} = \frac{\mathrm{G_\circ k_\circ \Phi}}{\sigma}\mathrm{e^{-\sigma N(HI,t)}} - \mathrm{R_f}\int_0^{\mathrm{r_{HI}}} \mathrm{n(r)n(HI)dr}, \tag{21}$$

where $\mathrm{r_{HI}}$ marks the depth of the pure HI layer. Using the relation $\mathrm{n(r)} = \mathrm{n_{ex}e^{N(r)/N_\circ}}$ ($\mathrm{N_\circ} = \mathrm{n_{ex}R}$) valid for a logotropic density profile, Eq. 21 eventually yields

$$\tau_\mathrm{f}\frac{\mathrm{d}\sigma\mathrm{N_{tr}(HI,t)}}{\mathrm{dt}} = \mathrm{r_{dis}e^{-\sigma N_{tr}(HI,t)}} - \sigma\mathrm{N_\circ}\left(\mathrm{e^{\sigma N_{tr}(HI,t)/\sigma N_\circ}} - 1\right). \tag{22}$$

where τ_f and $\mathrm{r_{dis}}$ are calculated with $\mathrm{n_{ex}}$. It can be easily seen that for $\mathrm{N_\circ} = \mathrm{n_{ex}R} \rightarrow \infty$ ($\mathrm{e^{N(HI,t)/N_\circ}} \rightarrow 1 + \mathrm{N(HI,t)/N_\circ}$), signifying a uniform density cloud $\mathrm{n} = \mathrm{n_{ex}}$ (or one with so large of a radius where the density of outer layers hardly changes), the latter reverts back to Eq. (14). Again we solve for $\mathrm{A_{FUV}^{(tr)}} = \sigma\mathrm{N_{tr}(HI,t)}$.

For $\mathrm{dA_{FUV}^{(tr)}(t)}/\mathrm{dt} \gg 0$ the solution of Eq. (22) remains the same as that of Eq. (14) with only $\mathrm{n_{ex}} = 2/3\langle\mathrm{n}\rangle$ replacing n. So in case of cloud destruction when $\mathrm{R_f} = 0$ Eq. (20) again gives the time dependence of the transition layer. In the case of $\mathrm{dA_{FUV}^{(tr)}(t)}/\mathrm{dt} \ll 0$, Eq. (22) is now approximated by ($\mathrm{A_\circ} = \sigma\mathrm{N_\circ}$)

$$\tau_\mathrm{f}\frac{\mathrm{dA_{FUV}^{(tr)}(t)}}{\mathrm{dt}} = -\mathrm{A_\circ}\left[\mathrm{e^{A_{FUV}^{(tr)}(t)/A_\circ}} - 1\right], \tag{23}$$

The solution of this being

$$\mathrm{A_{FUV}^{(tr)}(t) = A_\circ ln\left[1 + (e^{A_{FUV}^{(tr)}(0)/A_\circ} - 1)e^{-t/\tau_f}\right]} \quad (24)$$

The latter equation reduces to Eq. (18) when $\mathrm{N_\circ \to \infty}$ ($\mathrm{A_\circ \to \infty}$), as expected.

6.2.3 Collisional destruction of H_2 at high temperatures

At high temperatures the above is not a good description to follow the H_2 content. Once the temperature of the gas reaches $\mathrm{T_k \gtrsim 1000}$ K, H_2 formation effectively becomes zero (Cazaux & Tielens 2004). Moreover, at high temperatures the cloud scaling laws (and hence the expressions used to estimate $\mathrm{f_m}$) no longer hold since the observed "cloud" line widths would now be mostly thermal and thus no longer scale with size.

For temperatures above $\mathrm{T_k \gtrsim 3 \times 10^3}$ K the H_2 fraction will be controlled by collisional destruction processes according to

$$\mathrm{\frac{dn(H_2)}{dt} = -\gamma_1(T_k)n(H_2)n(HI) - \gamma_2[n(H_2)]^2}, \quad (25)$$

where $\mathrm{\gamma_1(T_k)}$ and $\mathrm{\gamma_2(T_k)}$ are the H_2-HI and H_2-H_2 collisional destruction coefficients. Their values can be found in Martin, Keogh, & Mandy (1998) where it can be seen that they are strongly temperature dependent($\propto T^{12}$). Also it turns out that the HI collisions are much more efficient in destroying H_2 than those with H_2 itself.

Indeed $\mathrm{[\gamma_1(T_k)/\gamma_2(T_k)]_{min} = 10}$ at $\mathrm{T_k \sim 3 \times 10^4}$ K and it is much bigger for lower gas temperatures. Thus for the H_2 collisions to be more important the condition

$$\mathrm{\frac{\gamma_2(T_k)[n(H_2)]^2}{\gamma_1(T_k)n(H_2)n(HI)} > 1 \Rightarrow \frac{n(H_2)}{n(HI)} > \frac{\gamma_1(T_k)}{\gamma_2(T_k)} \gtrsim 10.} \quad (26)$$

must be satisfied. In the WNM gas phase such a high percentage of remaining H_2 (remaining from the dominant FUV destruction mechanisms operating in the CNM, CNM-to-WNM phases) is unlikely. We thus consider only the HI collisional destruction term as important and then Eq. (25) becomes

$$\mathrm{\frac{dn(H_2)}{dt} = -\gamma_1(T_k)\,[n - 2n(H_2)]\,n(H_2)}, \quad (27)$$

where $\mathrm{n = n(HI) + 2n(H_2)}$ is the total density. Solving the latter eventually yields

$$\mathrm{f_m(t) = \frac{2n(H_2)}{n} = \frac{m_\circ e^{-n\gamma_1(T_k)t}}{1 - m_\circ e^{-n\gamma_1(T_k)t}}, \ \ \text{where} \ \ m_\circ = \frac{f_\circ}{1 - f_\circ}}. \quad (28)$$

The value $\mathrm{f_\circ}$ is the last value that $\mathrm{f_m}$ has before conditions change so that we switch to Eq. (28) to describe the evolving HI/H_2 equilibrium. Here we must mention that we assumed that in the WNM phase there is no FUV-induced HI/H_2 spatial segregation. If there is some remnant spatial segregation H_2 would be destroyed by the much less effective H_2 collisions, thus our assumption may somewhat overestimate the level of collisional H_2 destruction.

We now have all ingredients to build a H_2 formation module into numerical code for the simulation of the ISM of galaxies. Given the local conditions in the ISM we can follow the HI/H_2 transition using Eqs (14) or (22) for gas with $T < 1000$ K. Above 1000 K, it is $\mathrm{R_f} = 0$ and in this case these equations describe the photo-destruction of clouds. For $\mathrm{T} > 3000$ K, Eq. (28) is used as a rough approximation of the collisional destruction process. We have implemented a module using the above prescription in an N-body/SPH code that includes a detailed model for the neutral phases. We will estimate the local H_2 content using a sub-grid model calculating the solution to the time dependent Eq. (14) at every particle position in our simulation. Before we detail the precise algorithm we will first give some background of the code.

6.3 Implementation

The code we use is an N-body/SPH code for the simulation of galaxy sized objects. Details of the code are explained in previous chapters. Here we will use the complete model for the ISM described in Chapter 2 ("model D"). The main features of the code that make it especially attractive to follow the formation and destruction of molecular gas is the fact that our code includes an extensive ISM model as well as star formation and feedback. The ISM model lets the gas cool down to temperatures of $\mathrm{T} \leq 100$ K and the densities that are reached are of order $\mathrm{n} \approx 100$ cm^{-3}. As we will discuss below this is just the ISM phase we expect the transition to molecular gas to occur.

N-body/SPH codes are in routine use within the astrophysical community as tools to explore problems of galaxy evolution and formation and a description of this method can be found elsewhere (Hernquist & Katz 1989, Monaghan 1992). We use the conservative SPH formulation of Springel & Hernquist (2002). We employ a model for the WNM and CNM that was extended from Gerritsen & Icke (1997) and Bottema (2003). We will summarise the most important features here.

6.3.1 Neutral ISM model

Our model for the ISM is similar to the equilibrium model for the CNM and WNM of Wolfire et al. (1995, 2003). We solve for the ionization and thermal evolution of the gas including the various processes given in Table 6.1. An overview of the ISM model is given in Fig. 6.2, where we have plotted the equilibrium temperature, ionization fraction and pressure as a function of density. The plots in this figure show that as density varies, the equilibrium state of the gas changes from a high temperature/high ionization state ($\mathrm{T} = 10^4$ K, $\mathrm{x_e} \approx 0.1$) at low densities, to a low temperature/low ionization state ($\mathrm{T} < 100$ K, $\mathrm{x_e} < 10^{-3}$) at high densities. In between there is a density domain where the negative slope of the P-n relation indicates that the gas is unstable to isobaric pressure variations, the classic thermal instability (Field 1965). The shape of these curves and hence the exact densities of the thermal instability vary locally throughout the simulation under the influence of the local time-varying UV radiation field and supernova heating. We assume a constant cosmic ray ionization rate ζ_{CR} throughout the galaxy. We take a value of $\zeta_{\mathrm{CR}} = 3.6 \times 10^{-17}$ s^{-1}.

The FUV luminosities of the stellar particles, which are needed to calculate the local FUV field used in the photoelectric heating and that also will be used to calculate

Table 6.1: Overview of the processes included in the ISM model used. For H and He ionization equilibrium is explicitly calculated, for other elements collisional ionization equilibrium (CIE) is assumed. references: 1) Wolfire et al. 1995, 2) Raga et al. 1997 , 3) Verner & Ferland 1996, 4) Silva & Viegas 2001

process	comment	ref.
heating		
Cosmic Ray	ionization rate $\zeta_{\rm CR} = 3.6\ 10^{-17}$ s^{-1}	1
Photo Electric	FUV field from stars	1
cooling		
e, H_0 impact	H,He,C,N,O,Si,Ne,Fe	2,4
ionization		
& recombination		
UV	ionization assumed for species with $E_i < 13.6$ eV	
Cosmic Ray	H, He only; primary & secondary ionizations	1
Collisional	H, He only	3
Radiative recombination	H, He only	3
CIE	assumed for metals	

H_2 destruction, are derived from Bruzual & Charlot (1993, and updated) population synthesis models for a Salpeter initial mass function (IMF) with cutoffs at $0.1\ {\rm M}_\odot$ and $100\ {\rm M}_\odot$. In the present work we do not account for dust extinction of UV light, except for the fact that young stars are shrouded in their natal cloud: for young stellar clusters we decrease the amount of UV extinction from 75% to 0% in 4 Myr (Parravano et al. 2003).

6.3.2 Star formation and feedback

The coldest and densest phase in our model is best identified with the CNM, where giant molecular clouds are embedded and form. We use a simple prescription for star formation, based on the assumption that star formation is governed by the gravitational stability in the GMCs. A region is considered unstable to star formation if the local Jeans mass ${\rm M_J}$ is smaller than a reference mass ${\rm M_c}$. The rate of star formation is set to scale with the local free fall time:

$$\tau_{\rm sf} = {\rm f_{sf}} {\rm t_{ff}} = \frac{\rm f_{sf}}{\sqrt{4\pi {\rm G}\rho}} \tag{29}$$

The delay factor ${\rm f_{sf}}$ is uncertain, as we will discuss below this factor may influence the amount of H_2 formed. We will take values ranging from ${\rm f_{sf}} = 2.5 - 20$. The actual efficiency of star formation is then determined by the balance between the cooling of the gas and the UV and SN heating. Note that our star formation does not depend on the formation of molecular gas. This is reasonable as in this picture star formation is a process associated with collapse through self-gravity and, though in practice always

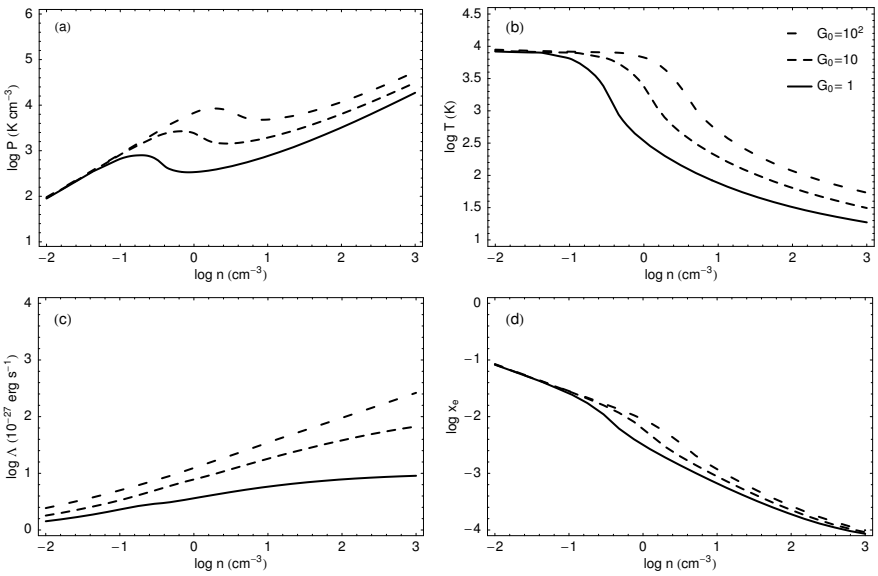

Figure 6.2: Overview of the ISM model: Equilibrium plots of (a) pressure P, (b) temperature T, (c) cooling rate Λ and (d) electron fraction $\mathrm{x_e}$ as a function of density n for three different values of the UV field $\mathrm{G_0}$ (given in units of 1.6×10^{-3} erg cm^{-2} s^{-1})

related to H_2 formation, it is independent of the gas phase. A "sanity" check on our model is thus simply to see if substantial star formation happens in regions with low H_2 content.

Feedback from stellar winds and supernovae is essential for regulating the ISM. While the mechanical energy output of stars is reasonably well known, it has proven to be difficult to include it completely self-consistently in galaxy sized simulations of the ISM. The reason for this is that the effective energy of feedback depends sensitively on the energy radiated away in thin shells around the bubbles created. This will mean that the effect of feedback is not reliable unless prohibitively high resolution is used. In SPH codes there have been conventionally two ways to account for feedback: by changing the thermal energy input and by acting on particle velocities. Both are unsatisfactory, as the thermal method suffers from over cooling (Katz 1992) and the kinetic method seems to be too efficient in disturbing the ISM (Navarro & White 1993). Here we use a new method based on the creation at the site of young stellar clusters of a *pressure particle* that acts as a normal SPH particle in the limit of the mass of the particle $\mathrm{m} \rightarrow 0$, for constant energy. For the energy injection rate we take $\dot{\mathrm{E}} = \epsilon_{\mathrm{sn}} \mathrm{n_{sn}} \mathrm{E_{sn}} / \Delta \mathrm{t}$, with $\mathrm{E_{sn}} = 10^{51}$ erg, $\epsilon_{\mathrm{sn}} = 0.1$, $\mathrm{n_{sn}} = 0.009$ per $\mathrm{M_\odot}$ and $\Delta \mathrm{t} = 3 \times 10^7$ yr. The efficiency ϵ_{sn} thus assumes that 90% of the energy is radiated away, a value which comes from more detailed simulations of the effect of supernova and stellar winds on the ISM (Silich et al. 1996), and is also used in other simulations of galaxy evolution (e.g. Semelin & Combes 2002, Springel & Hernquist 2002,

Buonomo et al. 2000). The feedback model is explained in more detail in chapter 3.

6.3.3 H_2 formation

For our H_2 formation model we follow the same philosophy as for the star formation model: unresolved structure is assumed to be present at the SPH particle positions. In this case the underlying cloud structures are assumed to conform to the relation (12) for the mean cloud extinction, derived from the observed density/size scaling relation (10). However, this equation is not expected to be valid everywhere in our simulation domain. Regions where Eq. (10) will fail are those with low density and pressure. In those regions our algorithm as detailed in section 6.2 will not give sensible outcomes. To be specific, if pressure is low, Eq. (10) predicts very large cloud sizes, such that the resulting photo-destruction of H_2 proceeds very slowly. To circumvent this problem we modify Eq. (10) for pressures below $\mathrm{P_{trans}}$:

$$\langle \mathrm{n} \rangle = \mathrm{n_o} \left(\frac{\mathrm{P_{trans}/k_B}}{10^4 \text{ K cm}^{-3}} \right)^{-1/2} \left(\frac{\mathrm{P_e/k_B}}{10^4 \text{ K cm}^{-3}} \right) \mathrm{R_{pc}^{-1}}, \tag{30}$$

where we take $\mathrm{P_{trans}} \approx 1000$ K cm^{-3}. This is just a convenient patch, which however in low pressure environments does scale the "clouds" according to the $\mathrm{n_{ex}} \propto \mathrm{P_e}$ scaling appropriate for diffuse clouds (Elmegreen 1993), and with this minor modification we can apply the sub-grid model to all ISM conditions.

For the macroscopic pressure $\mathrm{P_e}$ that enters in Eq. (12) we need the local velocity dispersion σ_{vel}. For this velocity dispersion we take the formal SPH estimate

$$\sigma_{\mathrm{j}}^2 = \sum_{\mathrm{i}} \frac{\mathrm{m_i}}{\rho_{\mathrm{j}}} (\mathrm{v_i} - \langle \mathrm{v} \rangle_{\mathrm{j}})^2 \mathrm{W}(|\mathrm{r_{ij}}|, \mathrm{h_j}) \tag{31}$$

with $\mathrm{v_i}$ and $\mathrm{m_i}$ the particle velocities and masses, $\langle \mathrm{v} \rangle_{\mathrm{j}}$ the local bulk velocity. A number of subtle issues are connected with the choice of the dispersion. Eq. (31) describes the interparticle velocity dispersion, while the dispersion that enters in the pressure (13) is really an inter-cloud velocity dispersion. Even if we assume these to be equivalent, the problem remains that Eq. (31) samples a velocity dispersion on scales of the smoothing lengths $\mathrm{h_i}$. We can try to account for this by scaling σ_{j}, using for example the relation for Kolmogorov turbulence,

$$\sigma'_{\mathrm{j}} = \sigma_{\mathrm{j}} \left(\frac{\mathrm{h_j}}{\mathrm{R_{cloud}}} \right)^{-1/3}, \tag{32}$$

but in practice this has very little influence on H_2 formation.

Depending on the cloud model assumed, Eq. (14) or (22) then describes the evolution of the HI layer during a simulation time step dt, given an initial $\mathrm{A_{FUV}^{(tr)}}$. The density that enters is assumed to be the mean density $\langle \mathrm{n} \rangle$ given by the SPH density at the particle position, and the temperature the particle temperature (both taken constant for the time step). The radiation field is calculated from the distribution of stars, where the assumption is that extinction from dust, or from molecular clouds is not important (apart from extinction from the natal cloud). After we have evolved the transition $\mathrm{A_{FUV}^{(tr)}}$ for the time step dt the resulting $\mathrm{f_m}$ (Eqs (8) and (9)) is calculated

and assigned to the SPH particle for the duration of the next time step (where it can be used to calculate for example cooling). At the next time step this value is retained and used to calculate the initial $\mathrm{A}_{\mathrm{FUV}}^{(\mathrm{tr})}$, given the new average cloud extinction $\langle \mathrm{A_v} \rangle$. The $\langle \mathrm{A_v} \rangle$ may have changed from the previous time step, if for example the pressure $\mathrm{P_e}$ has changed. The choice to keep $\mathrm{f_m}$ constant rather than $\mathrm{A}_{\mathrm{FUV}}^{(\mathrm{tr})}$ is dictated by $\mathrm{H_2}$ mass conservation, and the decision to assign all variations of $\mathrm{f_m}$ to the time varying UV field.

6.4 Application to a dwarf galaxy model

Our first application and test of the $\mathrm{H_2}$ formation model will be a model for a dwarf irregular galaxy. There are a number of practical reasons to choose this type of system as a test model, as well as some interesting questions particular to the $\mathrm{H_2}$ gas presence in dwarf galaxies that can be explored using our model.

Firstly, the small sizes of these systems allow relatively high resolution with modest computational effort. In our present work the choice of dwarf galaxies as modelling templates allows a given numerical simulation to probe small physical scales and high gas densities, the latter being of crucial importance if the HI→$\mathrm{H_2}$ phase transition is to be incorporated successfully. Insight gained from simulating these systems, whose properties are constrained by a wealth of observational data (e.g. van Zee 2001; Barone et al. 2000; de Paz et al. 2003), furthermore it holds the promise of yielding good constraints about physical processes that are expected to be universal in galaxies (as we have done for SN feedback strength; see Pelupessy et al. 2004).

Aside from being excellent testbeds for quantifying phenomena expected to be common across the Hubble sequence, dwarf galaxies are important systems on their own right because of their crucial role in current galaxy formation theories as the building "blocks" of larger systems (Kauffmann, White, & Guiderdoni 1993), and as major "polluters" of the intergalactic medium with metals (Ferrara & Tolstoy 2000).

6.4.1 Simulation setup

We construct a simple model of a dwarf irregular with gas mass of $\mathrm{M_{gas}} = 10^8\ \mathrm{M_\odot}$ and a stellar mass of $\mathrm{M_{star}} = 10^8\ \mathrm{M_\odot}$. The dark halo is constructed with a flat core, in agreement with Burkert (1995).

Specifically, the gas disk has radial surface density profile

$$\Sigma = \Sigma_\mathrm{g}/(1 + \mathrm{R}/\mathrm{R_g}), \tag{33}$$

with central density $\Sigma_\mathrm{g} = 10\ \mathrm{M_\odot/pc^2}$ and radial scale $\mathrm{R_g} = 0.33$ kpc, truncated at 4 kpc. An exponential stellar disk,

$$\rho_\mathrm{disk}(\mathrm{R}, \mathrm{z}) = \frac{\Sigma_0}{2\mathrm{h_z}} \exp(-\mathrm{R}/\mathrm{R_d}) \mathrm{sech}^2(\mathrm{z}/\mathrm{h_z}) \tag{34}$$

with central surface density $\Sigma_0 = 300\ \mathrm{M_\odot/pc^2}$, $\mathrm{R_d} = 0.5$ kpc and vertical scale height $\mathrm{h_z} = 0.2$ kpc, is constructed as in Kuijken & Dubinski (1995). The ages of the initial population of stars are distributed according to a constant SFR and an age of 13 Myr.

We take a halo profile

$$\rho_{\rm halo}({\rm r}) = \rho_0 \frac{\exp(-{\rm r}^2/{\rm r}_{\rm c}^2)}{1+{\rm r}^2/\gamma^2} \tag{35}$$

with core radius $\gamma = 2$ kpc, cutoff radius ${\rm r_c} = 20$ kpc and central density $\rho_0 = 2\times10^7\ {\rm M_\odot/kpc^3}$, for a total mass of ${\rm M_{halo}} = 15\times10^9{\rm M_\odot}$ and a peak rotation velocity of about 50 km/s. We represent the dark halo by a static potential.

6.4.2 Practical considerations

For H_2 to be able to form in the simulation two requirements must be met: we must probe in our simulation the gas densities where H_2 is expected to form, and at these densities stars must not form before H_2 has had a chance to form, as star formation will inhibit H_2 formation by irradiating and heating the gas. We can derive some minimum requirements in order for our model to be able to follow the HI→H_2 transition as well as some constraints on the ${\rm f_{sf}}$ star formation parameter. In addition, it may be necessary to consider the effect of H_2 cooling.

The necessary resolution, the choice of ${\rm M_{ref}}$

Simulations of self-gravitating fluids done with insufficient numerical resolution can suffer from artifacts: artificial clumping or inhibition of gravitational collapse may occur. For SPH simulations including self-gravity these effects can arise if the local Jeans mass is not resolved (Bate & Burkert 1997, Whitworth 1998). Hence, this requires for our simulation that

$${\rm M_J} \equiv \frac{\pi\rho}{6}\left(\frac{\pi{\rm s}^2}{{\rm G}\rho}\right)^{3/2} > {\rm N m_{SPH}}, \tag{36}$$

with s the sound speed, N the number of SPH neighbours and ${\rm m_{SPH}}$ is the particle mass. For our simulation, this requirement is met by a choosing the parameters of our star formation recipe such that violation of (36) is precluded by star formation. A gas particle will spawn star particles, and thus be subjected to heating that raises its Jeans mass, if ${\rm M_J} < {\rm M_{ref}}$. Taking ${\rm M_{ref}} \approx {\rm N m_{SPH}}$ the particle mass ${\rm m_{SPH}}$ will then determine the densities probed by the simulation. In figure 6.1 we can see that densities in the order of $50-100\ {\rm cm^{-3}}$ are sufficient to follow the HI→H_2 transition, while somewhat higher densities may be necessary for low metallicity gas. For such densities and typical CNM temperatures of 100 K Eq (36) corresponds to a Jeans mass of $\approx 10^4{\rm M_\odot}$, well below the typical GMC mass scales. Hence, running the simulation with particle masses of ${\rm m_{SPH}} \approx 500{\rm M_\odot}$ allows a good resolution of the aforementioned mass scale.

The choice of ${\rm f_{sf}}$: the role of H_2 and star formation

In our star formation recipe the delay for star formation to occur is set by the free parameter ${\rm f_{sf}}$. We will examine various values for this parameter and its effect on H_2 formation. It may seem somewhat odd that this parameter could determine whether

H_2 formation can happen, normally one views H_2 formation as a prerequisite for star formation, but remember that in our simulation these two are not causally linked.

We can use the timescale for the formation of H_2 along with the well-established empirical fact that everywhere in the local Universe stars seem to form out of molecular clouds rather than atomic gas to deduce a lower limit on the value of f_{sf}. For H_2 formation to remain always ahead of star formation it must be $\tau_f(H_2) \leq \tau_{sf}$, which from Eqs 2 and 29 becomes,

$$f_{sf} \gtrsim 5.33 \left(\frac{\langle n \rangle}{cm^{-3}}\right)^{-1/2} \left(\frac{\mu Z}{3.5}\right)^{-1} \left[\frac{(1+T/100\ K)^2}{(T/100\ K)^{1/2}}\right]. \quad (37)$$

Since CNM HI gas is the most likely precursor phase of the H_2 gas, for typical CNM conditions of $T_k \sim (100-200)$ K and $\langle n \rangle \sim (10-50)$ cm^{-3}, the latter equation yields $f_{sf} \gtrsim 3-10$. These values are roughly similar to those deduced using the constraints on the observed star formation rate in the Galaxy. Given the uncertainties inherent in e.g. the $S_H(T_k)$ function, such a rough agreement is noteworthy and here it is worth mentioning that $\tau_f(H_2)$ is also a good approximation of chemical equilibrium timescales in FUV-illuminated clouds (e.g. Hollenbach & Tielens 1999). Thus the rough agreement of the constraint set by Eq. 37 with what are considered reasonable f_{sf} values may signify an important role for cloud chemistry in setting the average star formation rate. This is not far-fetched since molecule formation enables totally different cooling functions for the gas and thus drastically alters its thermodynamic state allowing to eventually cool and fragment further (e.g. Chièze & Pineau des Forêts 1987).

Cooling by H_2

A recent calculation of the cooling by H_2 was done by Le Bourlot et al. (1999). At high and intermediate temperatures ($1000-8000$ K) H_2 is a more efficient coolant than the major coolants of atomic gas (C and Fe). Hence even a low (10^{-4}) remnant abundance of molecular gas in the diffuse WNM can have an impact on the cooling at high temperatures. Indeed some people have included H_2 cooling in their cooling curves, but without calculating the abundance of molecules (Carraro et al. 1998). Admittedly our accuracy in following the amount of warm molecular gas is limited, but to get some idea of the possible effect of this warm molecular gas it is nevertheless interesting to do some calculations including H_2 cooling. For this we use the Le Bourlot cooling curve, where we use a limited set of data (low density limit, constant ortho to para ratio, only H_2-H collision excitation), appropriate for our purposes. Note that some observations find abundances of H_2 gas the order of $10^{-4}-10^{-3}$ in diffuse HI gas, even in regions of the ISM hostile to H_2 formation, like galactic high velocity clouds (Richter et al. 2001).

6.5 Results for the dwarf galaxy model

In a model that incorporates H_2 formation the two most important parameters that should be explored are the formation rate μ and the metallicity Z. The formation rate is uncertain by a factor of 5-10, and this obviously introduces some uncertainty in the

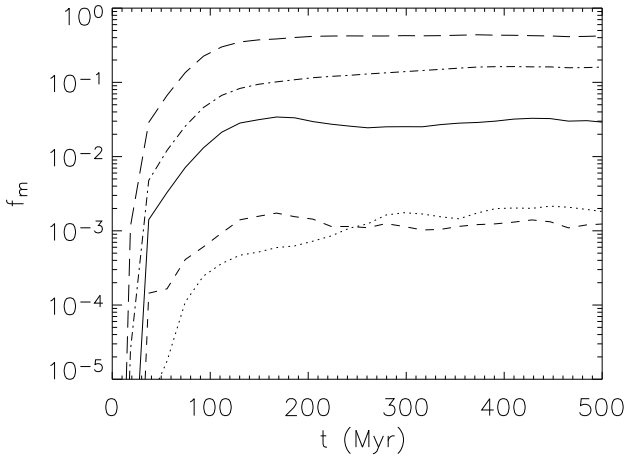

Figure 6.3: H_2 fraction. The lines indicate the time dependence of the molecular fraction f_m for different values of Z and μ. With, from top to bottom, **long-dashed line:** $\mu = 17.5, \mathrm{Z} = \mathrm{Z}_\odot$, **dash-dotted line:** $\mu = 17.5, \mathrm{Z} = \mathrm{Z}_\odot/5$, **drawn line:** $\mu = 3.5, \mathrm{Z} = \mathrm{Z}_\odot$, **Dashed line:** molecular fraction $\mathrm{f_m}$ for $\mu = 3.5, \mathrm{Z} = \mathrm{Z}_\odot/5$, and **Dotted line:** $\mu = 3.5, \mathrm{Z} = \mathrm{Z}_\odot/5$ with logotropic clouds. Simulations are started with $\mathrm{f_m} = 0$.

theoretically calculated H_2 content. For high formation rates large amounts of warm and diffuse H_2 may be present in the outer parts of spiral galaxies (Papadopoulos et al. 2002). Metals play an important role: the H_2 formation rate is directly proportional to the dust surface available, and we take this surface to be proportional to Z. Dust also plays an important role shielding molecules from UV radiation. Observations of low metallicity systems, like dwarf irregulars, using CO as a tracer give low molecular gas contents (e.g. Barone et al. 2000). However, the interpretation of these observations are complicated by the fact that the conversion factor from CO flux to H_2 mass under these conditions may not be reliably known: for low metallicity environments not enough C may be present to build self-shielding CO cores (Israel 1997).

Hence, we explore a small 2x2 grid of models using a formation rate of $\mu = 3.5$ and $\mu = 17.5$, and metallicities of either $\mathrm{Z} = \mathrm{Z}_\odot/5$ or $\mathrm{Z} = \mathrm{Z}_\odot$. Note that for our model dwarf galaxy the high metallicity is somewhat unrealistic, because normally dwarf galaxies have lower metal content. We included this to explore H_2 formation under conditions more pertinent to other systems. Note also that for simulations without H_2 cooling our sub-grid model only follows the H_2 content as a passive tracer of the history of the local conditions, thus the simulations for high and low formation rate will be identical except for the amount of H_2.

6.5.1 Spatial and temporal distribution of H_2 gas

We start the simulation with a gas disk that has a temperature of $\mathrm{T} \approx 8000$ K, and with a molecular fraction $\mathrm{f_m} = 0$. After the start of the simulation the gas cools and collapses on itself in the z-direction, forming regions of cold and dense gas in the

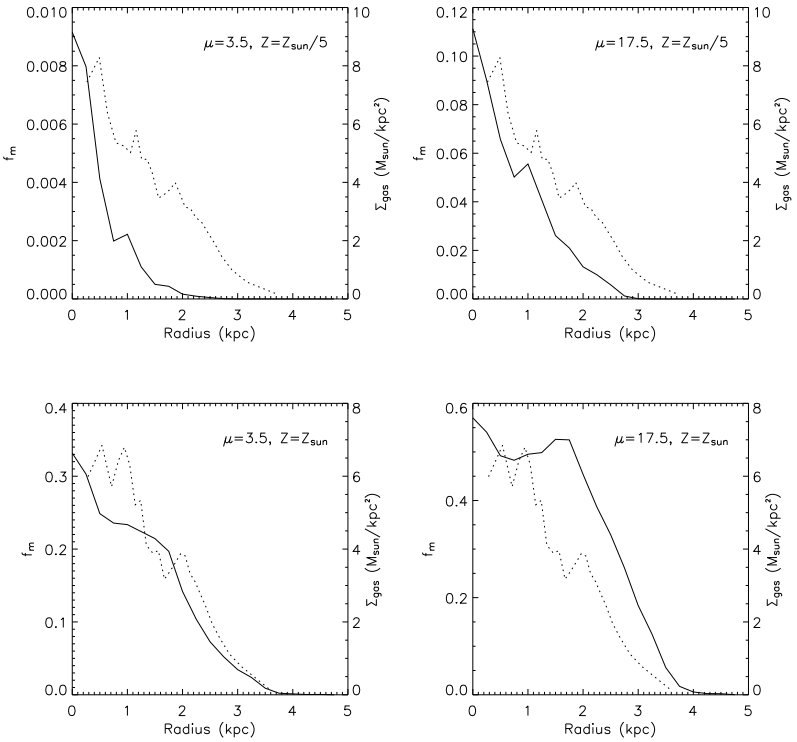

Figure 6.4: Radial dependence of the molecular fraction. **Drawn line:** mean molecular fraction as a function of radius (scale on left y-axes), and **dotted line:** total gas surface density (scale on right y-axes). Note that the y-axis scales are not the same for the different panels.

midplane. There, H_2 starts to form and after some time star formation starts taking place as well. An equilibrium fraction of H_2 is reached (Fig. 6.3) on a timescale of $\approx 50 - 100$ Myr. This agrees with our earlier estimate of Eq. (2). For this model galaxy, the mean star formation rate (SFR) is about $\mathrm{SFR} = 0.002\ \mathrm{M}_\odot/\mathrm{yr}$ for low Z and $\mathrm{SFR} = 0.003\ \mathrm{M}_\odot/\mathrm{yr}$ for high Z, with modest variations that cause some variations in $\mathrm{f_m}$, visible also in Fig. 6.3.

Furthermore we see that, as expected, the low μ/ low Z simulation has the lowest equilibrium molecular fraction of about $\mathrm{f_m} = 0.001$. A higher formation rate μ will boost that to $\mathrm{f_m} = 0.03$ for $\mu = 17.5$. For high metallicities, molecular fractions of $\mathrm{f_m} = 0.17$ ($\mu = 3.5$) and $\mathrm{f_m} = 0.4$ ($\mu = 17.5$) form. Also drawn in Fig. 6.3 is time dependence of the molecular fraction for a low μ/low Z simulation with logotropic clouds. As can be seen the difference between constant density and logotropic clouds is not very large, certainly smaller than the differences due to the formation rate parameter (this is also evident in the equilibrium $\mathrm{f_m}$ shown in the panels in Fig.6.1, where the main difference between constant density and logotropic clouds was that for logotropic clouds small fractions $\mathrm{f_m}$ remain at low densities).

In Figs. 6.4 and 6.5 we have plotted the (mean) molecular fraction as a function

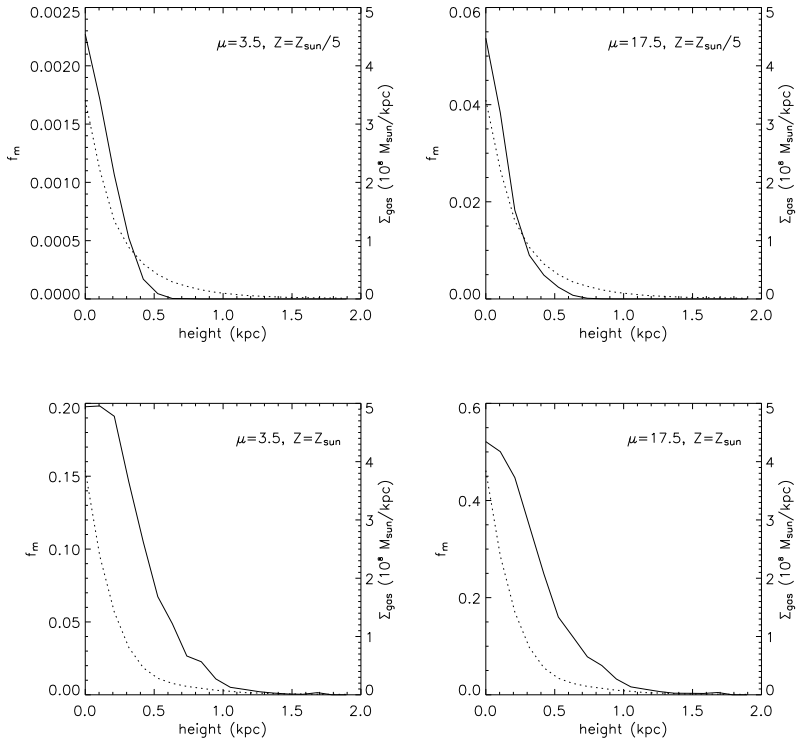

Figure 6.5: z-Height dependence of the molecular fraction. **Drawn line:** mean molecular fraction as a function of height above the disk plane (scale on left y-axes), and **dotted line:** total gas mass distribution (scale on right y-axes). Note that the y-axis scales are not the same for the different panels.

of radius and height above the disk-plane for the four simulations. We see that, as expected, molecules form mostly in the central regions and in the midplane. Note also that for high metallicity and high formation rate the molecular fraction seems to have a tendency to "saturate" in the central regions at a fixed value, in this case $\mathrm{f_m} = 0.6$.

Looking in more detail at the spatial distribution of H_2, Fig. 6.6, we see that H_2 is concentrated in the dense clumps and filaments of the HI distribution. Note also that if we compare the low and high μ simulations, we see that the distribution is similar: *the uncertainty in the formation parameter is mainly an uncertainty in the amount of H_2 formed, not in the locations of H_2 formation*. The relative distribution of H_2 is represented by our simulation, but the exact amount of H_2 is more difficult to determine exactly, as this depends on the formation rate parameter (as we will discuss further on, comparison with observations to constrain μ is not straightforward). If we look at the high metallicity simulations, we can see that, apart from the clumpy distribution there is also a sizable mass of "diffuse" H_2, where H_2 is more widespread, but still mainly confined to gas filaments.

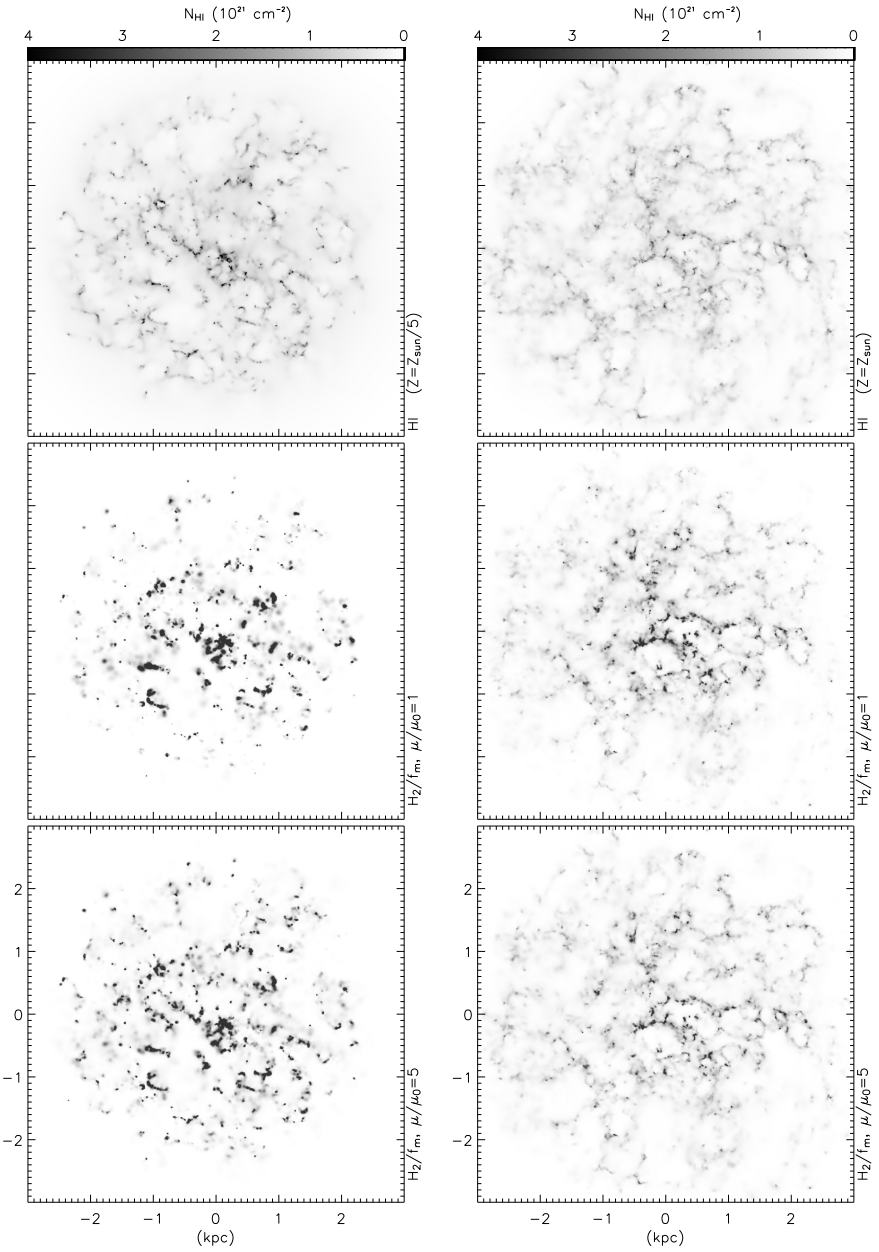

Figure 6.6: HI and H_2 maps. **Left panels:** results for $Z = Z_\odot/5$, **right panels:** $Z = Z_\odot$. Shown are, from top to bottom, the HI distribution, the H_2 distribution for $\mu = 3.5$ and for $\mu = 17.5$. The HI maps of low and high μ simulations are very similar, shown are only the maps for $\mu = 3.5$. The H_2 maps have been divided by the global molecular fraction such that the differences with the HI distribution can be seen more clearly.

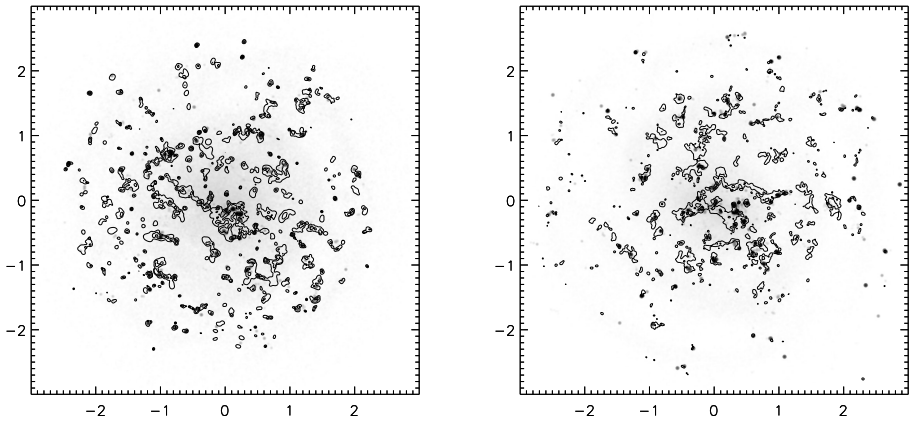

Figure 6.7: Hα and H_2: simulated Hα maps (greyscales) with H_2 contours. Left panel shows the maps for the $Z = Z_\odot/5$, $\mu = 3.5$ simulation (contours at column densities of $N_{HI} = 2\times10^{19}$ and 10^{20} cm^{-2}) while the right panel shows the $Z = Z_\odot$, $\mu = 17.5$ run (contours at column densities of $N_{HI} = 2 \times 10^{20}$ and 10^{21} cm^{-2}).

Finally we look at the relation between star formation and H_2. In Fig. 6.7 we have plotted a simulated map of "Hα" (actually a map of the luminosity of the stars in ionizing photons), overplotted with contours of H_2 gas. The contours are chosen such that the plots show the relation of star formation with the densest parts of the H_2 distribution. As can be seen star formation is almost always associated with some nearby complex of H_2 gas, while some H_2 clumps do not show Hα emission, these have not yet formed stars.

6.5.2 The influence of the collapse time

Apart from the parameters directly related to H_2 formation, f_m will also depend on the delay factor f_{sf}. As discussed in section 6.3.2, this parameter accounts for the fact that a region unstable to star formation does not collapse in the free-fall time τ_{ff}. The fact that we have time-dependent H_2 formation means that the total amount of H_2 is sensitive to the time regions stay in a cold and dense phase conducive to molecule formation. Indeed, comparing models run with different values for f_{sf}, we see that the total amount of molecular gas is strongly dependent on this parameter (Fig. 6.8). In our model the formation of stars and the formation of molecules are in competition. Thus we cannot make the delay factor too small as this would completely quench molecule formation. As we discussed in section 6.4.2, the chosen typical values of f_{sf}, as constrained by the observed H_2 mass in GMCs and the star formation rate in e.g. the Galaxy, satisfy Eq. 37 and thus H_2 formation always precedes star formation.

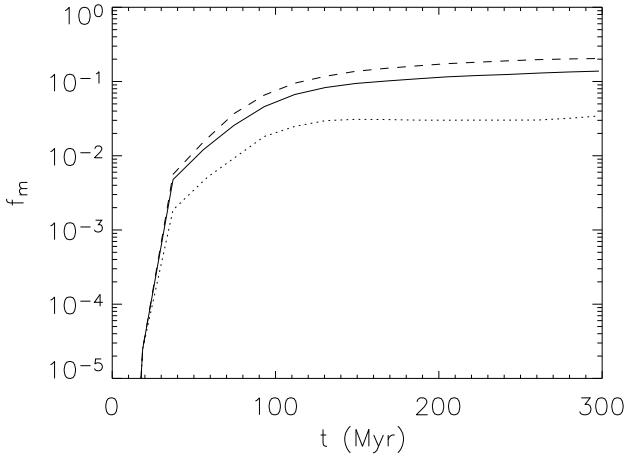

Figure 6.8: H_2 fraction vs time for simulations with different f_{sf}. **Dotted line:** $f_{sf} = 2.5$, **drawn line:** $f_{sf} = 10$, **dashed line:** $f_{sf} = 20$ (for all three: $\mu = 3.5$ and $Z = Z_\odot$).

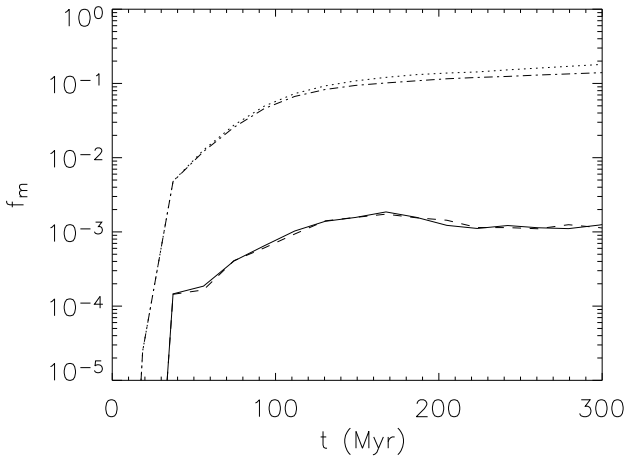

Figure 6.9: H_2 fraction vs time for simulations with cooling. **Drawn line:** $Z = Z_\odot/5$, **dashed line:**$Z = Z_\odot/5$ with H_2 cooling, **dash-dotted line:** $Z = Z_\odot$ and **dotted:** $Z = Z_\odot$ with H_2 cooling. For all: $\mu = 3.5$.

6.5.3 Simulations with H_2 cooling

The inclusion of the cooling by H_2 affects the simulation in a number of ways. As an extra coolant it will increase the amount of gas in a cold state. This in turn will increase the formation of H_2. However, star formation may also increase, and thus also the UV field. In Fig. 6.9 the effect of cooling on $\mathrm{f_m}$ is illustrated for the $\mu = 3.5$ simulations . As can be seen, cooling has only some influence for the high Z simulation. For the low Z simulation the molecular fractions are too low to substantially alter the results. Note that while H_2 is a strong coolant at high temperatures (of a few thousand K), where it will dominate the cooling for $\mathrm{f_m} > 0.001$, the effect of the extra cooling is limited because of the small amount of gas at these temperatures.

6.5.4 Discussion

Detection and mapping of the molecular component of dwarf galaxies is usually done by mapping of the $^{12}\mathrm{CO(J = 1 \rightarrow 0)}$ line (e.g. Barone et al. 2000, Mizuno et al. 2001) or by UV absorption studies (Tumlinson et al. 2002). The derived H_2 fractions are in the order of 1-10 percent, but for low metallicity systems CO is often not detected giving only upper limits for the molecular fraction in the order of a percent. A direct comparison with our simulations must be made cautiously because our simulations do not follow the formation of CO, in fact we cannot probe the state of gas where the formation of CO will take place, because of the high densities and low temperatures needed. Hence we cannot determine CO luminosity directly, although in principle empirical relations for the ratio $\mathrm{M_{H_2}/L_{CO}}$, the so-called $\mathrm{X_{CO}}$ factor, as a function of $\mathrm{G_0}$ and Z could be used to derive expected CO brightness distributions (Israel 1997). Nonetheless, the molecular fractions we derive seem to be reasonable, although for low μ/ low Z the derived fraction of $\mathrm{f_m}$ is rather low. This could indicate that a higher formation rate is likely. The molecular fraction may increase somewhat for a simulation run at higher resolution, because in metal poor environments the HI$\rightarrow$$H_2$ transition is taking place above $\mathrm{n = 100\ cm^{-3}}$, this can increase $\mathrm{f_m}$ by a factor 2-5.

For the galaxy models run with high metallicity and/or formation rate we find quite substantial fractions of H_2, of $\mathrm{f_m} = 0.17 - 0.4$. However we also find suprisingly high values, $\mathrm{f_{H_2}} \approx 0.001 - 0.01$, of the diffuse warm neutral medium to be molecular. To illustrate this we have plotted in Fig.6.10 the molecular fraction as a function of total column density for a face-on projection. There is a clear column density threshold for the presence of H_2 for the low metallicity simulation. For high metallicity even low column density regions (which are also of low density and high temperature) show fractions of $\mathrm{f_{H_2}} \approx 0.001 - 0.01$. We can compare this to studies done with the Far Ultraviolet Spectroscopic Explorer (Tumlinson et al. 2002), where typical upper limits of $\mathrm{f_m} \leq 10^{-6}$ are found for such low column density regions. Furthermore the state of the gas (low density, high temperature) is also not typically associated with the presence of such quantities of molecular gas. There is no - or very little - formation of molecular gas going on in this gas phase and any H_2 present should dissociate. In fact, destruction is taking place in the simulation, but the timescales of destruction are quite long. For the thermal dissociation this is due to the low density of the gas: for temperatures of $\mathrm{T = 5000\ K}$ and density of $\mathrm{n_H = 0.3\ cm^{-3}}$ the collisional destruction timescale (for neutral gas) is still $\tau_{\mathrm{col}} \approx 10^8$ yr. Furthermore, for

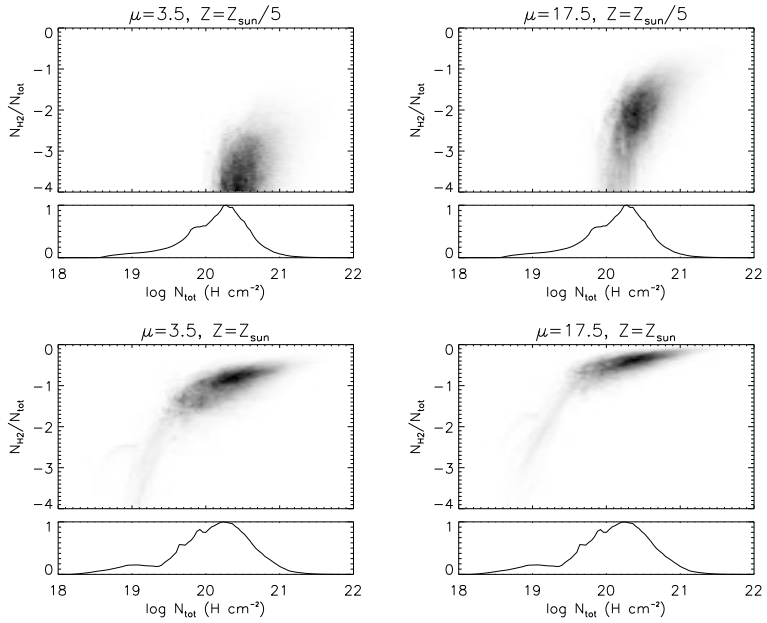

Figure 6.10: Fraction of H_2 vs total column densities.

our model galaxy the radiation fields in quiescent regions are quite low, $\mathrm{G}_0 \lesssim 0.1$, due to the low star formation, so the radiative dissociation timescales are also in the order $\tau_{\rm rad} = 1.3/\mathrm{G}_0 \times 10^7$ yr$\approx 10^8$ yr. So we see that the fact that H_2 can survive some time in lukewarm gas is not unrealistic. Note however that the simulation may not represent the dispersion of H_2 from dense regions realistically: molecular gas is formed in star forming regions, where radiation fields are higher (for our model up to $\mathrm{G}_0 = 100$). As the star formation heats the surrounding gas it will destroy H_2, the amount of molecular gas that "escapes" destruction is then sensitive to for example the time it is exposed to the high radiation field or the combination of high density/ high temperature. Also, destruction by supernova shocks is not represented very well, because the interaction of the supernova shocks with the (sub resolution) molecular clouds is absent. Nevertheless, our simulations indicate that in so far as the molecular gas is not destroyed, it will survive and so the warm medium of quiescent dwarf galaxies may still contain significant amounts of H_2. More active galaxies will destroy H_2 effectively by UV irradiation. Note that for similar reasons H_2 in the outer regions of spiral galaxies may survive for long times. This result may indicate the origin of the H_2 rotational emission from the disk of NGC891, where an extended and pervasive component of warm H2 with a scale length larger than that of the cooler molecular gas traced by CO was found (Valentijn & Van der Werf 1999). This warm H_2 can then by identified with the warm, extended, moderate density transition zones between GMCs and the WNM, and trace amounts of H_2 in the WNM that has espaced destruction in relatively quiescent regions.

6.6 Conclusions

We have presented a method to calculate the local H_2 content in simulations of the ISM based on a subgrid model for the formation and destruction of molecular clouds. The model includes the formation of H_2 on dust grains and destruction of molecules by UV irradiation, including the effects of shielding by dust and self-shielding. Its main assumption is that the formation of H_2 takes place in structures that conform to observed density/size scaling relations, and that are present on scales not directly probed by the hydrodynamic code of the simulation. We presented steady state solutions of the model for the molecular fraction $\mathrm{f_m}$ as a function of the macroscopic density, temperature, velocity dispersion, radiation field, and metallicity. The effect of cloud substructure is roughly accounted for by taking $1/\mathrm{r}$ density profiles for the model clouds, but this has only modest effect on the derived H_2 fractions.

A simple time-dependent formulation of the same model can be coupled to hydrodynamic simulations, and thus calculate the local evolution of $\mathrm{f_m}$ according to the local macroscopic quantities. We have implemented the model in an N-body/SPH code for the simulation of galaxy sized objects. We applied this model to a model low surface brightness dwarf, and found the following:

- We found that our model reproduces reasonable molecular fractions ranging from $\mathrm{f_m} = 0.001 - 0.03$ for low metallicity systems to $\mathrm{f_m} = 0.17 - 0.4$ for solar metallicity.
- The biggest uncertainty is the exact value of the formation rate parameter μ adopted, however the general features of the H_2 spatial distribution do not depend on μ.
- The molecular fraction also shows a strong dependence on the metallicity Z. This is physically reasonable. However our model run for high metallicity shows surpising amounts of "diffuse" H_2, possibly due to the low radiation fields outside star forming regions. This may be analogous to what happens in the outer regions of spiral galaxies where the radiation field drops, and a diffuse H_2 gas phase may be present.
- Our model for molecular hydrogen is sensitive to details of our star formation recipe, as star formation controls the destruction of H_2.
- H_2 cooling has only a minor impact for our model.

Summarizing, we have developed an algorithm to calculate the evolution of the molecular phase of galaxies, coupled to the evolution of their gaseous and stellar components. Strong points are that it is simple, physically motivated and not computationally expensive. It is well suited to galaxy-sized simulations where a complete treatment of the physics involved in the formation of the H_2 clouds is not yet attainable, and in our case it complements our ISM description of the neutral phases. The astrophysical questions that it may be applied to include the question of the distribution and role of H_2 in irregular dwarf galaxies such as the LMC, where complete cloud surveys have recently become available. Also interesting would be application of the model to mergers of spiral galaxies, as observations show that large concentrations of

molecular gas are present in between the cores of the merging galaxies (e.g. Stanford et al. 1990), preceding or concurrent with the starbursts associated with these events. The concentrations of molecular gas are possibly forming out of the disrupted HI that "rushes" towards such regions. A direct example is furnished by the advanced merger NGC6240 (Van der Werf et al 1993), where the molecular gas is located between the remnant stellar nuclei. Here the strong emission from H2 in rotational and vibrational lines provides a direct measurement of the cooling radiation, showing that in extreme cases the additional cooling by molecular gas does play an important role. This effect is further enhanced by the suppression of [CII] $158\,\mu$m emission in these objects (e.g., Malhotra et al 1997), which is one of the principal coolers in more diffuse gas. Our model can be used to investigate the emergence of such a merger-induced molecular gas phase along with the evolving morphology and star formation rate. The fact that our prescripition takes account of the role of the macroscopic pressure for the formation of H_2 may be important for a complete understanding of this class of objects since the ISM pressure environment is expected to be rapidly evolving.

References

Abel, T., Anninos, P., Zhang, Y., & Norman, M. L., 1997, *New Astronomy* **2**, 181

Andersen, R.-P. & Burkert, A., 2000, *ApJ* **531**, 296

Barone, L. T., Heithausen, A., Hüttemeister, S., Fritz, T., & Klein, U., 2000, *MNRAS* **317**, 649

Bash, F. N., Green, E., & Peters, W. L., 1977, *ApJ* **217**, 464

Bate, M. R. & Burkert, A., 1997, *MNRAS* **288**, 1060

Blitz, L. & Shu, F. H., 1980, *ApJ* **238**, 148

Bottema, R., 2003, *MNRAS* **344**, 358

Bruzual A., G. & Charlot, S., 1993, *ApJ* **405**, 538

Buch, V. & Zhang, Q., 1991, *ApJ* **379**, 647

Buonomo, F., Carraro, G., Chiosi, C., & Lia, C., 2000, *MNRAS* **312**, 371

Burkert, A., 1995, *ApJ* **447**, L25+

Carraro, G., Lia, C., & Chiosi, C., 1998, *MNRAS* **297**, 1021

Cazaux, S. & Tielens, A. G. G. M., 2002, *ApJ* **575**, L29

Cazaux, S. & Tielens, A. G. G. M., 2004, *ApJ* **604**, 222

Chièze, J. P., 1987, *A&A* **171**, 225

Chièze, J.-P. & Pineau Des Forêts, G., 1987, *A&A* **183**, 98

Elmegreen, B. G., 1989, *ApJ* **338**, 178

Elmegreen, B. G., 1993, *ApJ* **411**, 170

Elmegreen, B. G., 2002, *ApJ* **577**, 206

Engargiola, G., Plambeck, R. L., Rosolowsky, E., & Blitz, L., 2003, *ApJS* **149**, 343

Ferrara, A. & Tolstoy, E., 2000, *MNRAS* **313**, 291

Field, G. B., 1965, *ApJ* **142**, 531

Gerritsen, J. P. E. & de Blok, W. J. G., 1999, *A&A* **342**, 655

Gerritsen, J. P. E. & Icke, V., 1997, *A&A* **325**, 972

Gil de Paz, A., Madore, B. F., & Pevunova, O., 2003, *ApJS* **147**, 29

Goldshmidt, O. & Sternberg, A., 1995, *ApJ* **439**, 256

Habart, H., Boulanger, F., Verstraete, L., Pineau des Forêts, G., Falgarone, E., & Abergel, A., 2000, in *ESA SP-456: ISO Beyond the Peaks*, pp 103–+

Habing, H. J., 1968, *Bull. Astron. Inst. Netherlands* **19**, 421

Helfer, T. T., Regan, M. W., Thornley, M. D., Wong, T., Sheth, K., Vogel, S. N., Bock, D. C.-J., Blitz, L., & Harris, A., 2001, *Ap&SS* **276**, 1131

Hernquist, L. & Katz, N., 1989, *ApJS* **70**, 419

Hidaka, M. & Sofue, Y., 2002, *PASJ* **54**, 223

Hollenbach, D. J. & Tielens, A. G. G. M., 1999, *Rev. of Mod. Phys.* **71**, 173

Hollenbach, D. J., Werner, M. W., & Salpeter, E. E., 1971, *ApJ* **163**, 165

Honma, M., Sofue, Y., & Arimoto, N., 1995, *A&A* **304**, 1

Israel, F. P., 1997, *A&A* **328**, 471

Jura, M., 1974, *ApJ* **191**, 375

Jura, M., 1975, *ApJ* **197**, 575

Katz, N., 1992, *ApJ* **391**, 502

Katz, N., Furman, I., Biham, O., Pirronello, V., & Vidali, G., 1999, *ApJ* **522**, 305

Kauffmann, G., White, S. D. M., & Guiderdoni, B., 1993, *MNRAS* **264**, 201

Kuijken, K. & Dubinski, J., 1995, *MNRAS* **277**, 1341

Larson, R. B., 1981, *MNRAS* **194**, 809

Le Bourlot, J., Pineau des Forêts, G., & Flower, D. R., 1999, *MNRAS* **305**, 802

Li, W., Evans, N. J., Jaffe, D. T., van Dishoeck, E. F., & Thi, W., 2002, *ApJ* **568**, 242

Malhotra, S. et al., 1997, *ApJ* **491**, L27+

Martin, P. G., Keogh, W. J., & Mandy, M. E., 1998, *ApJ* **499**, 793

McLaughlin, D. E. & Pudritz, R. E., 1996, *ApJ* **469**, 194

Mihos, J. C. & Hernquist, L., 1994, *ApJ* **437**, 611

Mizuno, N., Yamaguchi, R., Mizuno, A., Rubio, M., Abe, R., Saito, H., Onishi, T., Yonekura, Y., Yamaguchi, N., Ogawa, H., & Fukui, Y., 2001, *PASJ* **53**, 971

Monaghan, J. J., 1992, *ARA&A* **30**, 543

Navarro, J. F. & White, S. D. M., 1993, *MNRAS* **265**, 271

Papadopoulos, P. P., Thi, W.-F., & Viti, S., 2002, *ApJ* **579**, 270

Parravano, A., Hollenbach, D. J., & McKee, C. F., 2003, *ApJ* **584**, 797

Pelupessy, F. I., van der Werf, P. P., & Icke, V., 2004, *A&A* **422**, 55

Pirronello, V., Liu, C., Shen, L., & Vidali, G., 1997, *ApJ* **475**, L69+

Raga, A. C., Mellema, G., & Lundqvist, P., 1997, *ApJS* **109**, 517

Regan, M. W., Thornley, M. D., Helfer, T. T., Sheth, K., Wong, T., Vogel, S. N., Blitz, L., & Bock, D. C.-J., 2001, *ApJ* **561**, 218

Richter, P., Sembach, K. R., Wakker, B. P., & Savage, B. D., 2001, *ApJ* **562**, L181

Semelin, B. & Combes, F., 2002, *A&A* **388**, 826

Silich, S. A., Franco, J., Palous, J., & Tenorio-Tagle, G., 1996, *ApJ* **468**, 722

Silva, A. I. & Viegas, S. M., 2001, *Computer Physics Communications* **136**, 319

Springel, V., 2000, *MNRAS* **312**, 859

Springel, V. & Hernquist, L., 2002, *MNRAS* **333**, 649

Stanford, S. A., Sargent, A. I., Sanders, D. B., & Scoville, N. Z., 1990, *ApJ* **349**, 492

Sternberg, A., 1988, *ApJ* **332**, 400

Stone, J. M., Ostriker, E. C., & Gammie, C. F., 1998, *ApJ* **508**, L99

Tumlinson, J. et al., 2002, *ApJ* **566**, 857

Vázquez-Semadeni, E., 2002, in *ASP Conf. Ser. 276: Seeing Through the Dust: The Detection of HI and the Exploration of the ISM in Galaxies*, pp 155–+

Valentijn, E. A. & van der Werf, P. P., 1999, *ApJ* **522**, L29

van der Werf, P. P., Genzel, R., Krabbe, A., Blietz, M., Lutz, D., Drapatz, S., Ward, M. J., & Forbes, D. A., 1993, *ApJ* **405**, 522

van Zee, L., 2001, *AJ* **121**, 2003

Verner, D. A. & Ferland, G. J., 1996, *ApJS* **103**, 467

Webber, W. R., 1998, *ApJ* **506**, 329

Wolfire, M. G., Hollenbach, D., McKee, C. F., Tielens, A. G. G. M., & Bakes, E. L. O., 1995, *ApJ* **443**, 152

Wolfire, M. G., McKee, C. F., Hollenbach, D., & Tielens, A. G. G. M., 2003, *ApJ* **587**, 278

Wong, T. & Blitz, L., 2002, *ApJ* **569**, 157

Yamaguchi, R., Mizuno, N., Onishi, T., Mizuno, A., & Fukui, Y., 2001, *PASJ* **53**, 959